Earth and Planetary Science Letters 445 (2016) 79–91

Contents lists available at ScienceDirect

Earth and Planetary Science Letters

www.elsevier.com/locate/epsl

Prolonged post-rift magmatism on highly extended crust of divergent continental margins (Baiyun Sag, South China Sea)

Fang Zhao [a,h,i], Tiago M. Alves [b], Shiguo Wu [c,*], Wei Li [d,c,*], Mads Huuse [e], Lijun Mi [f], Qiliang Sun [g], Benjun Ma [h,i]

[a] CAS Key Laboratory of Marginal Sea Geology, South China Sea Institute of Oceanology, Chinese Academy of Sciences, Guangzhou 510301, China
[b] 3D Seismic Lab. School of Earth and Ocean Sciences, Cardiff University, Main Building, Park Place, Cardiff, CF10 3AT, United Kingdom
[c] Institute of Deep-Sea Science and Engineering, Chinese Academy of Sciences, Sanya 572000, China
[d] Institute for Geosciences, University of Kiel, Kiel 24188, Germany
[e] School of Earth, Atmospheric and Environmental Sciences, University of Manchester, Manchester M13 9PL, UK
[f] Department of Exploration, CNOOC, Beijing 100010, China
[g] Key Laboratory of Tectonics and Petroleum Resources, China University of Geosciences, Ministry of Education, Wuhan 430074, China
[h] Key Laboratory of Marine Geology and Environment, Institute of Oceanology, Chinese Academy of Sciences, Qingdao 266071, China
[i] University of Chinese Academy of Sciences, Beijing 100049, China

ARTICLE INFO

Article history:
Received 27 January 2016
Received in revised form 30 March 2016
Accepted 1 April 2016
Available online xxxx
Editor: P. Shearer

Keywords:
South China Sea
continental margin
breakup sequence
magma
volcanic edifices

ABSTRACT

Three-dimensional (3D) seismic, borehole and geochemical data reveal a prolonged phase of post-rift magmatism on highly extended crust of the Baiyun Sag, South China Sea. Two volcanic complexes are identified and described in the context of continental rifting and diachronous continental breakup of the South China Sea. Biostratigraphic data from exploration wells BY7-1 and BY2, complemented by K–Ar datings from core samples, confirm that magmatic activity in the Baiyun Sag occurred in two main stages: (1) a first episode at the base of the Miocene (23.8 Ma); and (2) a second episode occurring at the end of the Early Miocene (17.6 Ma). The relative location of volcanic complexes in the Baiyun Sag, and their stratigraphic position, reveals prolonged magmatism inboard of the ocean–continent transition zone during continental breakup. We suggest that magmatism in the Baiyun Sag reflects progressive continental breakup in the South China Sea, with the last volcanic episode marking the end of a *breakup sequence* representing the early post-rift tectonic events associated with the continental breakup process. Seismic and borehole data from this *breakup sequence* records diachronous magma emplacement and complex changes in depositional environments during continental breakup.

© 2016 The Authors. Published by Elsevier B.V. This is an open access article under the CC BY-NC-ND license (http://creativecommons.org/licenses/by-nc-nd/4.0/).

1. Introduction

Divergent continental margins record along- and across-strike variations in the absolute values of crustal stretching (β), geometry of rift-related faults, and extent of magmatic activity (e.g. Lister et al., 1986; Reston, 2007; Huismans and Beaumont, 2008; Franke, 2013). Along-strike variations are documented in the form of contrasting subsidence histories of adjacent segments of divergent margins prior to, during, and after continental breakup, which is usually diachronous in the direction of ocean opening (Pindell et al., 2014). Magmatism can also vary in magnitude and extent, at places overprinting syn-rift topography to form vast regions with seaward-dipping reflections, or SDRs (Mutter et al., 1982). In other segments of the same margin, volcanism is sparse and associated with specific syn-rift structures, as in the case of West Iberia-Newfoundland (Manatschal and Bernoulli, 1999; Whitmarsh et al., 2001). Divergent continental margins are thus often classified as 'volcanic' or 'non-volcanic' (or magma-rich and magma-poor) depending on the relative expression of volcanism they present (White and McKenzie, 1989; Franke, 2013).

Recent interpretations take into account a wider spectrum of divergent margins in terms of their magmatic histories (Franke, 2013). In the South China Sea (SCS), spatial and temporal variations in rifting and continental breakup, and distinct syn-rift and post-rift histories across different crustal segments of the SCS, resulted in contrasting magmatic and subsidence histories (Franke, 2013). Comprising one of the largest marginal seas in the western Pacific (~3,500,000 km^2), the SCS records syn-rift and early post-rift extension in continental-slope basins (Li et al., 2013). Con-

* Corresponding authors.
E-mail addresses: swu@sidsse.ac.cn (S. Wu), li@geophysik.uni-kiel.de (W. Li).

http://dx.doi.org/10.1016/j.epsl.2016.04.001
0012-821X/© 2016 The Authors. Published by Elsevier B.V. This is an open access article under the CC BY-NC-ND license (http://creativecommons.org/licenses/by-nc-nd/4.0/).

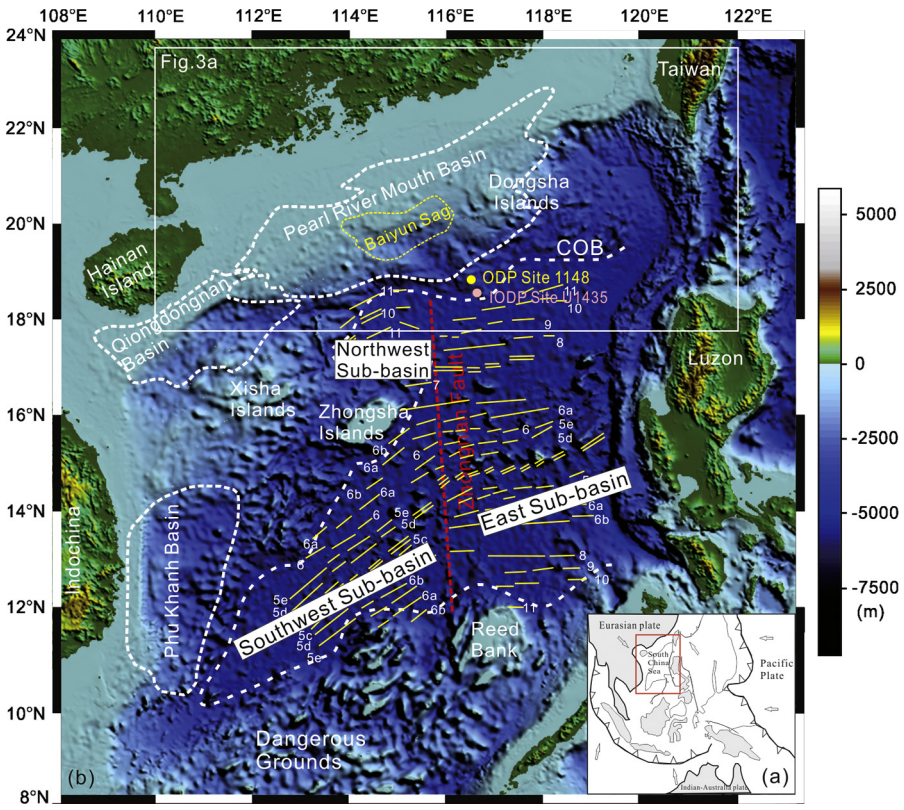

Fig. 1. Geological framework of the South China Sea region. (b) Location map showing the study area and main sedimentary basins in the South China Sea. The SCS consists of Northwest, East, and Southwest Sub-basins. The dashed white line is the continent–ocean boundary as defined by geophysical and drilling studies. Magmatic anomalies are from Briais et al. (1993). The locations of ODP Site 1148 and IODP Site U1435 are labelled in this figure. COB, continent–ocean boundary.

tinental breakup was diachronous across the SCS and associated with the propagation of seafloor spreading towards the southwest (Briais et al., 1993; Franke, 2013; Li et al., 2014) (Fig. 1b). Such a diachroneity in continental breakup resulted in a variety of ages for the breakup unconformity, each recording the onset of extension and breakup in distinct segments of the SCS (Fig. 2). To the northeast, close to Taiwan, a breakup unconformity was identified and correlated with a depositional hiatus between 37 Ma and 30 Ma (Lin et al., 2003). A correlative unconformity, dated as ~33 Ma at IODP Site U1435, represents the earliest regional seafloor spreading in the study area, and marks an important change in regional depositional settings (Li et al., 2014; Fig. 2). Another unconformity (~23.8 Ma) at ODP Site 1148 documents the onset of seafloor spreading in the Southwest Sub-basin (Wang et al., 2000; Li et al., 2014) (Fig. 2). The age of this unconformity fits well a breakup-related hiatus at 22–23 Ma recognised in the Qiongdongnan Basin (Zhou et al., 1995) (Fig. 2).

Acknowledging the existence of disparate syn- to post-rift evolutions on adjacent continental margins, Soares et al. (2012, 2014) proposed *breakup sequences* to comprise the complete seismic and stratigraphic expression of lithospheric breakup and associated tectonic movements. Soares et al. (2012) questioned this concept based on the discovery that rifting and final continental breakup occurred in two distinct stages of lithospheric stretching. The interpretation of *breakup sequences* involves the detailed recognition of unconformities (and their correlative surfaces) that bound strata deposited during the tectonic events associated with the continental breakup process, along distinct segments of a newly formed margin. In contrast, the classic definition of 'breakup unconformity' (e.g. Falvey, 1974) implies the generation, at the time of crustal breakup and onset of oceanic crust accretion, of a basin-wide unconformity between syn-rift and post-rift strata (e.g. Kyrkjebø et al., 2004; Whitmarsh and Wallace, 2001; Withjack et al., 1998).

In this work, 3D seismic interpretation techniques, borehole wireline and sidewall core data are used to examine the nature of volcanic mounds in the Baiyun Sag, a sub-basin of the PRMB, providing new insights on magma emplacement mechanisms in deep-water basins. In summary, this paper addresses the following research questions:

a) What is the importance and extent of volcanism inboard of the regions where continental breakup occurred in the northern SCS?
b) What is the timing of such volcanism in relation to rifting and continental breakup in the northern SCS?
c) What palaeobathymetric and subsidence histories are expected in the areas where important volcanism is observed during continental breakup?

2. Geological setting

The Baiyun Sag, located south of the PRMB, developed during the Early Paleogene to Early Miocene in association with continental rifting and seafloor spreading in the SCS (Sun et al., 2008; Li et al., 2013). The timing of seafloor spreading in the SCS has recently been revised using data collected at IODP Site U1435, from 33 Ma to 15 Ma in the Northeast Sub-basin, and from 23.6 Ma to 16 Ma in the Southwest Sub-basin (Li et al., 2014) (Fig. 2). Biostratigraphic, magnetic and subsidence data suggest that seafloor spreading in the SCS started during the Early Oligocene, before terminating in the Late Oligocene (Zhou et al., 1995; Taylor and Hayes, 1983; Li et al., 2014). In the deep-offshore Baiyun and Liwan Sags, local uplift events relate to the generation of a late Oligocene (30 Ma) unconformity. However, much younger

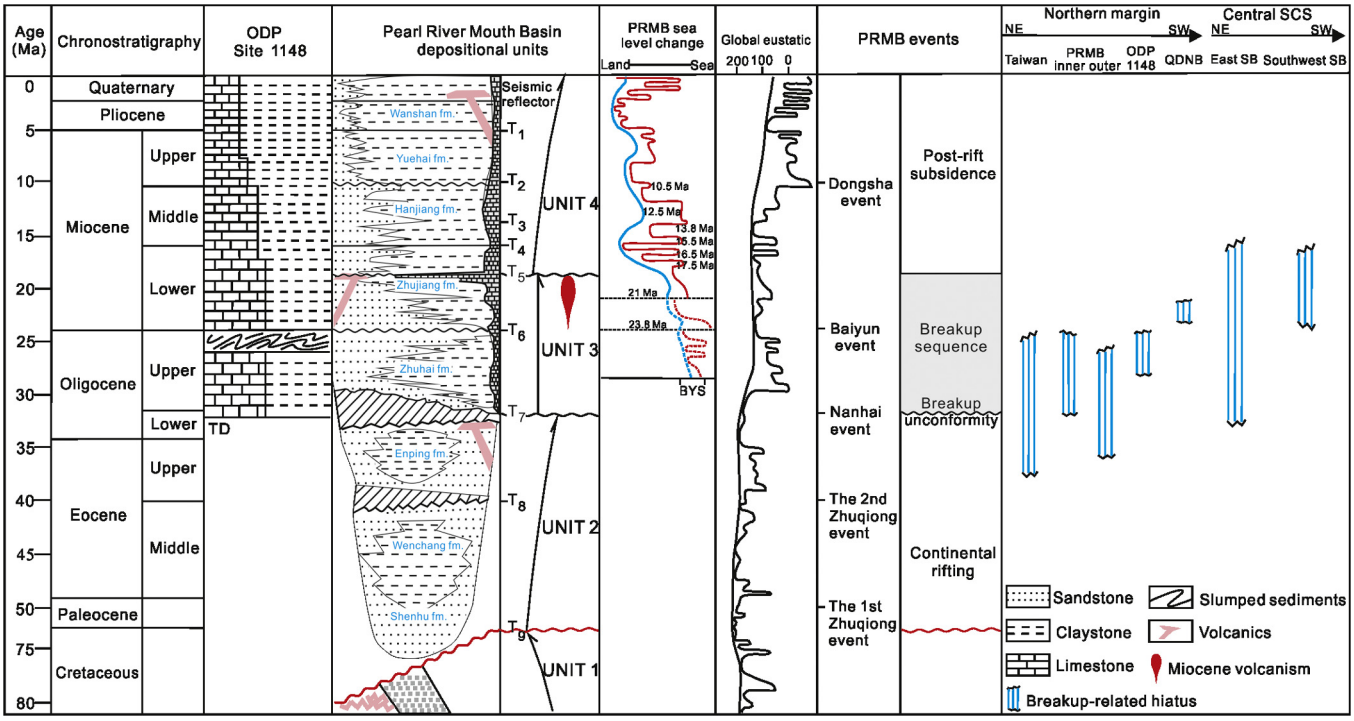

Fig. 2. Lithostratigraphic chart comparing the Pearl River Mouth Basin with strata crossed by ODP site 1148 (modified from Li et al., 2006). The table shows the main lithostratigraphic units and associated tectonic events in the study area, together with breakup-related hiatuses from the northern and central SCS (Lin et al., 2003; Zhou et al., 1995; Wang et al., 2000; Li et al., 2014; Taylor and Hayes, 1983; Franke, 2013). SB – Sub-basin; TD – total depth; fm – formation.

(Miocene) subsidence is still recorded in the Baiyun Sag in response to progressive continental breakup towards the southwest (Xie et al., 2014).

Inboard of the Baiyun Sag, the evolution of the PMRB records three main stages (Yu, 1994): (1) an early stage of continental rifting and onset of subsidence (Late Cretaceous–Early Oligocene); (2) a transitional stage recording widespread faulting, subsidence and deposition within distinct sub-basins (Late Oligocene–Early Miocene); and (3) a post-rift stage of basin infill occurring after the Early Miocene (Fig. 2). Outboard of the continental shelf, previous studies have revealed faulted crustal blocks typical of highly extended continental crust (Nissen et al., 1995; Hu et al., 2009; Lester et al., 2014). Following rifting, continental crust in the deep-offshore Baiyun Sag was thinned rapidly to <7 km under the rift axis, and a large number of low-angle faults were developed from the Early Oligocene (~32 Ma) to Late Miocene (~5.5 Ma), or even later (Hu et al., 2009; Sun et al., 2014a, 2014b).

This work considers continental breakup in the Baiyun Sag started during the Nanhai Event, which occurred at the Early Oligocene (Li et al., 2014; Sun et al., 2008; Fig. 2). The Baiyun Event took place at ~23 Ma, corresponding to a jump in ocean spreading from the Northeast to the Southwest Sub-basin (Sun et al., 2008; Fig. 1). A third tectonic pulse, the Dongsha Event occurred in the Late Miocene (10.5 Ma) and ceased around the Miocene/Pliocene boundary (5.5 Ma) (Lüdmann and Wong, 1999). As a result of this evolution, the Cenozoic succession in the Baiyun Sag comprises Eocene to Quaternary strata (Fig. 2).

Geological and geophysical studies have provided evidence for the moderate magmatism in the SCS, which exhibits characteristics of both magma-rich and magma-poor margins (Franke, 2013). Evidence of SDRs characteristic of magma-rich margins has not been found, but geophysical data (ESP, MCS and OBS) from the northern slope of SCS reveals a high velocity layer (HVL) in the lower crust. This HVL is likely related to underplating or magma emplacement, but the timing of this event is still uncertain (Fig. 3a) (Shi et al., 2005; Lester et al., 2014; Gao et al., 2015). In the Pearl River Mouth Basin (PRMB), there is widespread evidence for Cenozoic and Quaternary volcanism on borehole, gravity, magnetic and low-resolution 2D/3D seismic data (Fig. 3a). Initially, widespread magmatism occurred in the PRMB with a bimodal character between 64 and 32 Ma (Yan et al., 2006), i.e. before seafloor spreading began in the Northeast Sub-basin (Li et al., 2014). A second magmatic episode, Oligocene–Middle Miocene in age, resulted in widespread intrusion along faults, which fed mafic and intermediate extrusive material on a relatively small scale (Yan et al., 2006). Recently, a large number of Lower Miocene intrusive and extrusive edifices were identified throughout SCS e.g., at the PRMB, Phu Khanh Basin and offshore Taiwan, and were interpreted as post-rift magmatic bodies (Yan et al., 2006; Zhao et al., 2014; Sun et al., 2014a, 2014b; Lester et al., 2014) (Figs. 1b and 3a).

3. Data and methods

This study uses 3D seismic data acquired in the Baiyun Sag by the China National Offshore Oil Corporation (Fig. 3b). The interpreted 3D seismic volume covers an area of ~8000 km^2 in water depths of 100 m to 2500 m. Seismic acquisition used 3000-m long streamers with 240 channels, a geometry that produced a 3D seismic data with a bin size of 12.5 m. In this work, volcanic mounds are mapped using two-way travel time (TWT) structural and coherency maps. Coherency maps measure waveform similarity, i.e., how a trace is similar to its neighbouring traces (Brown, 2004). The coherence maps were based on the 'semblance method' of Hale (2013). In our work, semblances are computed from small numbers (3 in 2D, 3 × 3 1/4 9 in 3D) of adjacent seismic traces, by aligning traces so that coherent reflections become horizontal. In addition, the seismic-based method used in this paper takes into account the 'post-intrusion' distribution of sedimentary strata in the Baiyun Sag with onlapping terminations onto volcanic mounds, and forced folds above igneous complexes, constraining the relative timing of volcanism (e.g. Trude et al., 2003; Planke et al., 2005; Sun et al., 2014a, 2014b).

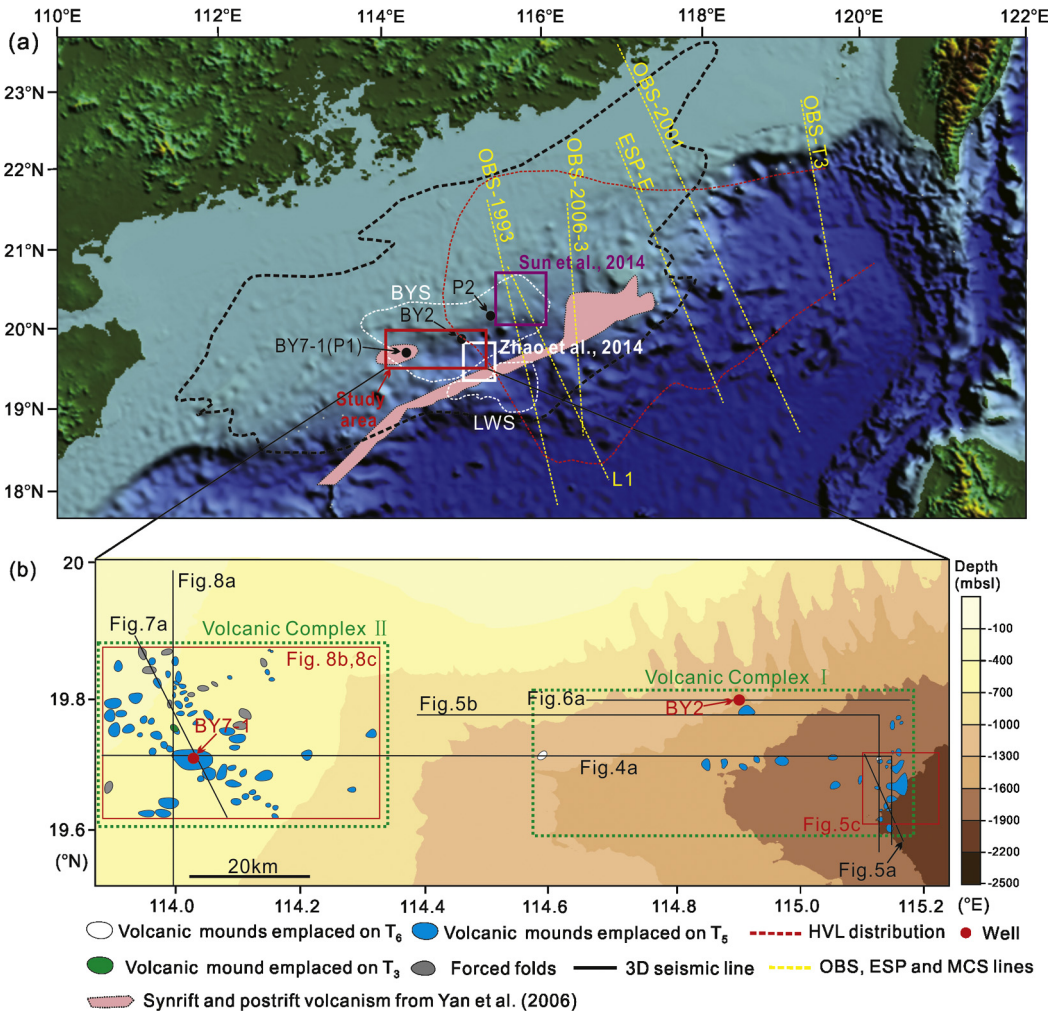

Fig. 3. (a) Overview map of the northern South China Sea showing main sedimentary sub-basins (BYS, LWS), syn-rift and post-rift volcanics identified in Yan et al. (2006). The study area is marked by the red box. The locations of boreholes BY7-1 and BY2 are labelled in the figure. Yellow dashed lines mark the locations of previous expanding spread profiles (ESP), ocean bottom seismograph (OBS) and multi-channel seismic (MCS) profiles (OBS-T3 from Lester et al. (2014); OBS-2001 from Wang et al. (2006); ESP-E are from Nissen et al. (1995). L1 from Gao et al. (2015) identified the high velocity layer (HVL) referred to in the text. The white and purple rectangles mark the location of igneous complexes identified in the Baiyun Sag. (b) Depth contour map of the seafloor illustrating the distribution of volcanic mounds in the study area. The locations of figures are labelled. Green dashed boxes highlight the location of Volcanic Complexes I and II. These two complexes have a NW–SE orientation and cover an area of approximately 3000 km^2. BYS – Baiyun Sag; LWS – Liwan Sag; ESP – expanding spread profile; MCS – multi-channel seismic profile; OBS – ocean bottom seismograph. (For interpretation of the references to colour in this figure legend, the reader is referred to the web version of this article.)

Borehole BY2 and BY7-1 drilled mudstones with an internal P-wave velocity of 2800 m/s around and above the imaged volcanic edifices. The dominant frequency of sediments surrounding the volcanic edifices is 35 Hz, resulting in a vertical resolution of 20 m. A measured interval P-wave velocity of 4500 m/s within the volcanic edifices implies a vertical seismic resolution of 32 m. An estimated P-wave velocity of 5500 m/s (Skogly, 1998) for the intrusive sills suggests a vertical seismic resolution of ~39 m. These values were used to calculate the depth of intrusive and extrusive igneous bodies.

Regional lithostratigraphic units interpreted in this work follow the nomenclature used by the China National Offshore Oil Corporation (CNOOC). Additional age and sedimentological information is based on samples collected in wells BY2 and BY7-1. As a result, eight major stratigraphic boundaries have been interpreted in the study area and named as T_g, T_7, T_6, T_5, T_4, T_3, T_2 and T_1 (Fig. 2).

4. Regional seismic stratigraphy

Seismic profiles and borehole data were used to interpret the seismic-stratigraphy of the Baiyun Sag (Figs. 4–8). We identified four main units: Unit 1 (oldest) to Unit 4 (youngest). These units correlate with distinct depositional environments and tectonic phases.

Units 1 to 4 are bounded by four regional unconformities (Figs. 4–8): (1) Horizon T_g marks the first identifiable unconformity and the top of the Mesozoic basement, (2) the Early Oligocene 'breakup unconformity' (T_7) records the onset of seafloor spreading on the northern margin of the SCS (Briais et al., 1993; Li et al., 2013; Franke, 2013), (3) the Late Oligocene–Early Miocene unconformity (T_6) represents the opening of the Southwest Subbasin (Wang et al., 2000; Li et al., 2014), and (4) Horizon T_5, which represents the top of volcanic complexes and carbonate intervals and comprises the regional unconformity marking the end of seafloor spreading.

4.1. Unit 1 (Pre-rift basement)

The Mesozoic Unit 1 is topped by Horizon T_g and is characterised by chaotic, discontinuous internal reflections. Unit 1 shows a deep erosional surface at its base (Figs. 4 and 8). The horizon (T_g) represents the top of pre-rift strata and forms the base of the wedge-shaped syn-rift strata. Unit 1 is composed of Lower Palaeozoic metamorphic rocks and Mesozoic igneous and sedimentary

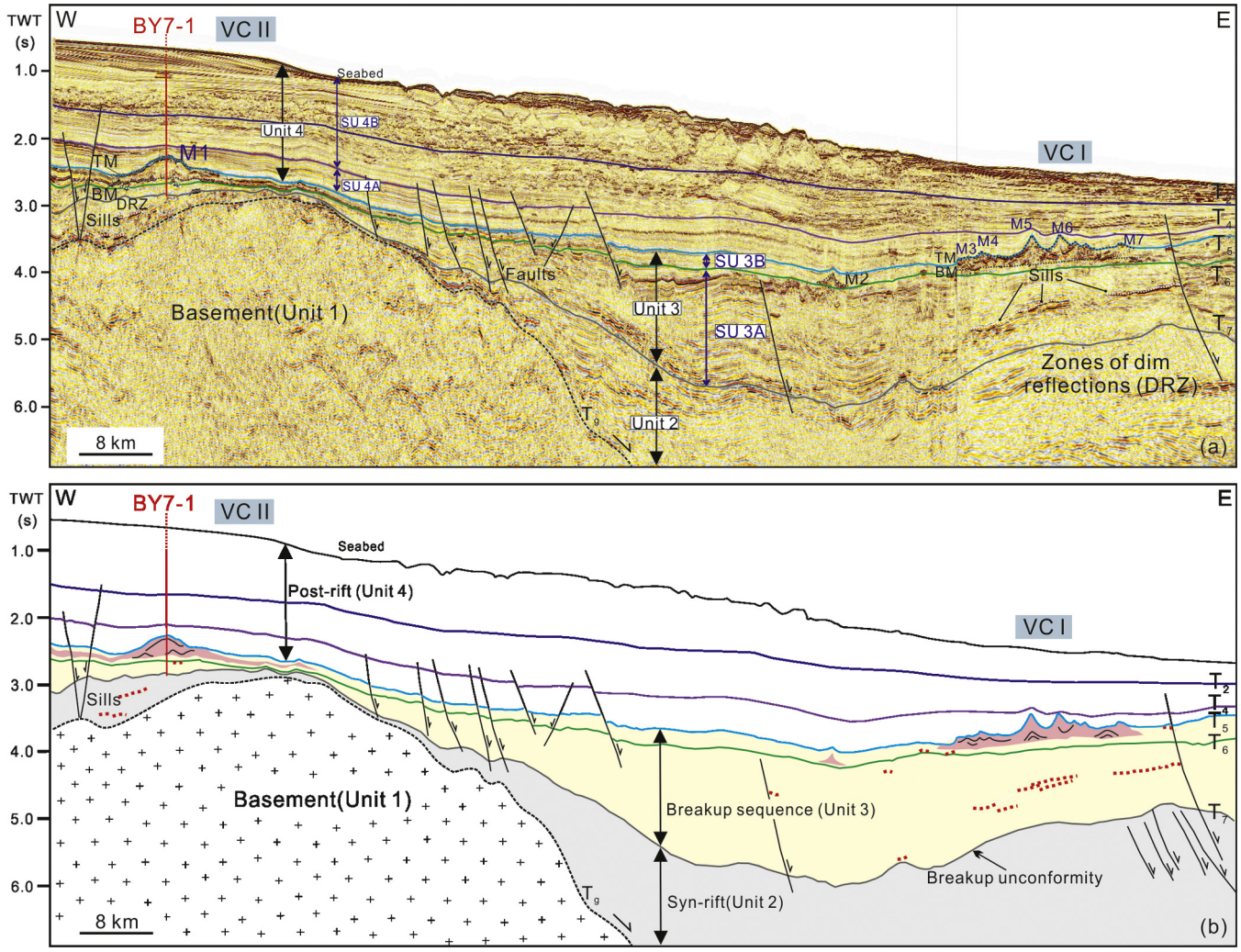

Fig. 4. (a) Regional seismic line showing intrusive and extrusive features in Volcanic Complexes I (VC I) and II (VC II). Key seismic horizons and seismic units are also shown. Horizons T_2, T_4 and T_6 correspond to the base of Upper Miocene, Middle Miocene and Lower Miocene strata, respectively. Well BY7-1 is shown as a red solid line penetrating mound M1. Note that mounded structures sit over two unconformities (T_6, T_5) and present variations in their height and diameter. (b) Schematic interpretation of (a) highlighting the location of igneous complexes in the Baiyun Sag. TM – top mound reflection; BM – base of mound; SU – Sub-unit. See location in Fig. 3b. (For interpretation of the references to colour in this figure legend, the reader is referred to the web version of this article.)

units, most of which were deposited in fluvial and lacustrine environments (Li and Rao, 1994; Fig. 2).

4.2. Unit 2 (Paleocene–Early Oligocene)

Unit 2 shows chaotic internal reflections, with variable amplitude, above the acoustic basement (Figs. 4, 6 and 8). Wedge-shaped seismic packages in Unit 2 tend to thin towards the footwall of basin-boundary faults (Figs. 4 and 8). These packages are interpreted as syn-rift strata. In the central part of the Baiyun Sag, Unit 2 is marked by sub-parallel seismic reflections (Figs. 4 and 6). Unit 2 onlaps the underlying basement and the flanks of basement highs (Figs. 4 and 8). Horizon T_7 bounds Unit 2 at the top and represents an Early Oligocene 'breakup unconformity' in the Baiyun Sag (Figs. 4–8).

Data from adjacent industry wells (Li and Rao, 1994) suggest a Paleocene to Early Oligocene age (65 to 32 Ma) for Unit 2, which comprises alluvial sands, shales and volcanic sequences (Shenhu Formation), followed by lacustrine shales intercalated with thin-bedded sandstones and siltstones (Wenchang Formation; Fig. 2). Fluvial-lacustrine shales and sandstones also occur within Unit 2, as part of the Enping Formation (Li and Rao, 1994). Altered vitric-lithic tuffs and basaltic ash, dated as 35.5±2.8 Ma (early Oligocene to late Eocene), were drilled by well BY7-1 (Fig. 7).

4.3. Unit 3 (Late Oligocene-earliest Miocene)

Unit 3 is bounded at its base by a 'breakup unconformity' (T_7) and at its top by volcanic complexes and carbonate intervals drilled by wells BY2 and BY7-1 (Horizon T_5; Figs. 4–8). Its base (T_7) onlaps and drapes syn-rift strata in Unit 2. Borehole data shows the top of Unit 3 as marking an important change in depositional environments within the Baiyun Sag, from shallow-marine to open marine depositional environments (Figs. 6 and 7).

Based on its seismic character and geometry, Unit 3 is clearly not uniform in the Baiyun Sag. Thus, in this study we subdivide Unit 3 into sub-units 3A and 3B, which in effect comprise two distinct seismic packages separated by T_6 (Figs. 4–8). Horizon T_6 comprises a ~23 Ma unconformity at wells BY2 and BY7-1 and at ODP Site 1148. It is recognised as a moderate to high-amplitude horizon with relatively good continuity (Figs. 4–8).

Sub-unit 3A shows parallel to sub-parallel internal reflections with low to moderate amplitude, and semi-discordant igneous sills of high-amplitude (Figs. 4–8). The sedimentary rocks forming this

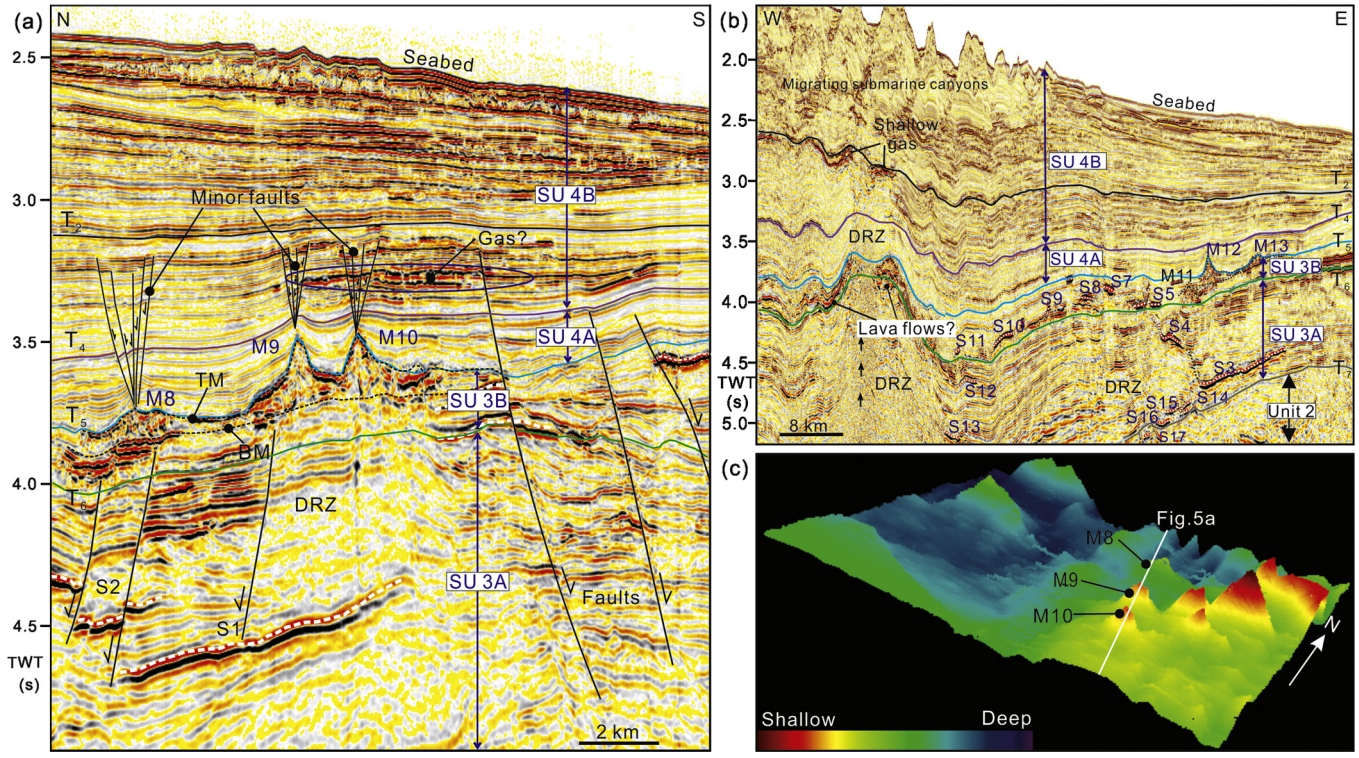

Fig. 5. 3D seismic profiles showing Volcanic Complex I in detail. See locations in Fig. 3b. In (a) and (b), mounded structures (M8 to M13), igneous sills (S1 to S17), zones of dim reflections (DRZ) and shallow gas are labelled. Horizon T_5 coincided with the top of Volcanic Complex I. Seventeen igneous sills are imaged in this area as concordant or "transgressive" intrusions. (c) Three dimensional visualisation of Horizon T_5 highlighting the structural alignment of mounds in the Baiyun Sag.

unit comprise Upper Oligocene deltaic to marginal marine sandstones, with shales, volcanics and limestones (Fig. 2). In well BY2, sub-unit 3A includes Oligocene volcanic rocks towards its upper part (Fig. 6). In well BY7-1, sub-unit 3A is recognised by the occurrence of intrusive dolerites at 2845 m below the seafloor (Fig. 7).

Sub-unit 3B comprises a series of volcanic complexes and interbedded carbonates crossed by wells BY2 and BY7-1 (Figs. 6 and 7). Carbonates likely accumulated in shallow-marine environments (~5–30 m), but alternate with deeper and sub-aerial facies, a character suggesting multiple pulses of relative sea-level rise and fall. The time interval during which the volcanic complexes and limestones were formed correlates with the opening of the Southwest Sub-basin. Similar unconformities topped by carbonate deposits have been documented on both northern and southern SCS margins, namely in the western PRMB, the northern Dongsha Islands, the Qiongdongnan Basin, Dangerous Grounds and the Reed Bank area (Fig. 1b; Ding et al., 2015).

In the Baiyun Sag, the sedimentary environment changed from shallow- to deep-marine after the Early Miocene unconformity (T_5) (Fig. 3). Units 2 and 3 thicken towards the northeast, accompanying the observed deepening of the Baiyun Sag in the same direction (Figs. 1b and 4).

4.4. Unit 4 (late Early Miocene to Holocene)

Unit 4, late Early Miocene to Holocene in age, can be subdivided into two seismic sub-units (Figs. 4–8). It lies directly on the top of volcanic complexes and carbonate intervals in Unit 3 (Figs. 4–8). Its base is coincident with Horizon T_5, a prominent unconformity occurring at the top of the interpreted volcanic complexes. An age of ~18 Ma is inferred for Horizon T_5 based on stratigraphic data from well BY7-1.

Sub-unit 4A is characterised by continuous parallel reflections of low to moderate amplitude, which often onlaps the underlying sub-units 3A and 3B (Figs. 4–8). Sub-unit 4A (Lower Miocene) comprises muddy sandstones and siltstones, with minor amounts of claystones (Fig. 7). On borehole data is also observed a finning-upwards trend in Unit 4A, suggesting a progressive rise in sea level towards its upper part (Fig. 7).

Sub-unit 4B spans the Middle Miocene to Holocene and shows continuous, moderate- to high-amplitude reflections (Figs. 4 to 8). It changes into chaotic, transparent reflections with variable amplitude towards its top (Figs. 4 to 8). Strata forming this unit are composed of claystones and siltstones with minor sandstones (Fig. 7). Seismic data interpreted along the northern slope of Baiyun Sag reveal the presence of migrating submarine canyons within sub-unit 4B, and sediment drifts deposited by strong deep-water currents (Figs. 5 and 6).

5. Morphology of volcanic complexes

5.1. Volcanic Complex I

Mounded features in Volcanic Complex I are observed in the central part of the Baiyun Sag (Fig. 3). The interpreted 3D seismic data reveal 28 mounded structures and numerous high amplitude acoustic anomalies in this first complex (Figs. 3b and 4). The mounded structures have diameters of 0.5 km to 3.0 km, heights of 240 m to 840 m, and flank dips of 10° to 32° (Figs. 4 and 5). At their base, the mounds correspond to a locally discontinuous, low- to high-amplitude positive reflection (BM), which is sub-parallel to the underlying strata (Figs. 4 and 5). The mounds are bounded at their tops by a moderate- to high-amplitude positive reflection (TM) that is onlapped by strata in sub-unit 4A (Figs. 4 and 5). Figs. 4 and 5 highlight the complex, and often chaotic, internal seismic character of the mounds downlapping onto horizon BM. Most of the mounds occur above "acoustically dim" zones. Other mounds are developed close to the upper tips of faults, which extend downwards into the deeper strata (Figs. 4 and 5). Gen-

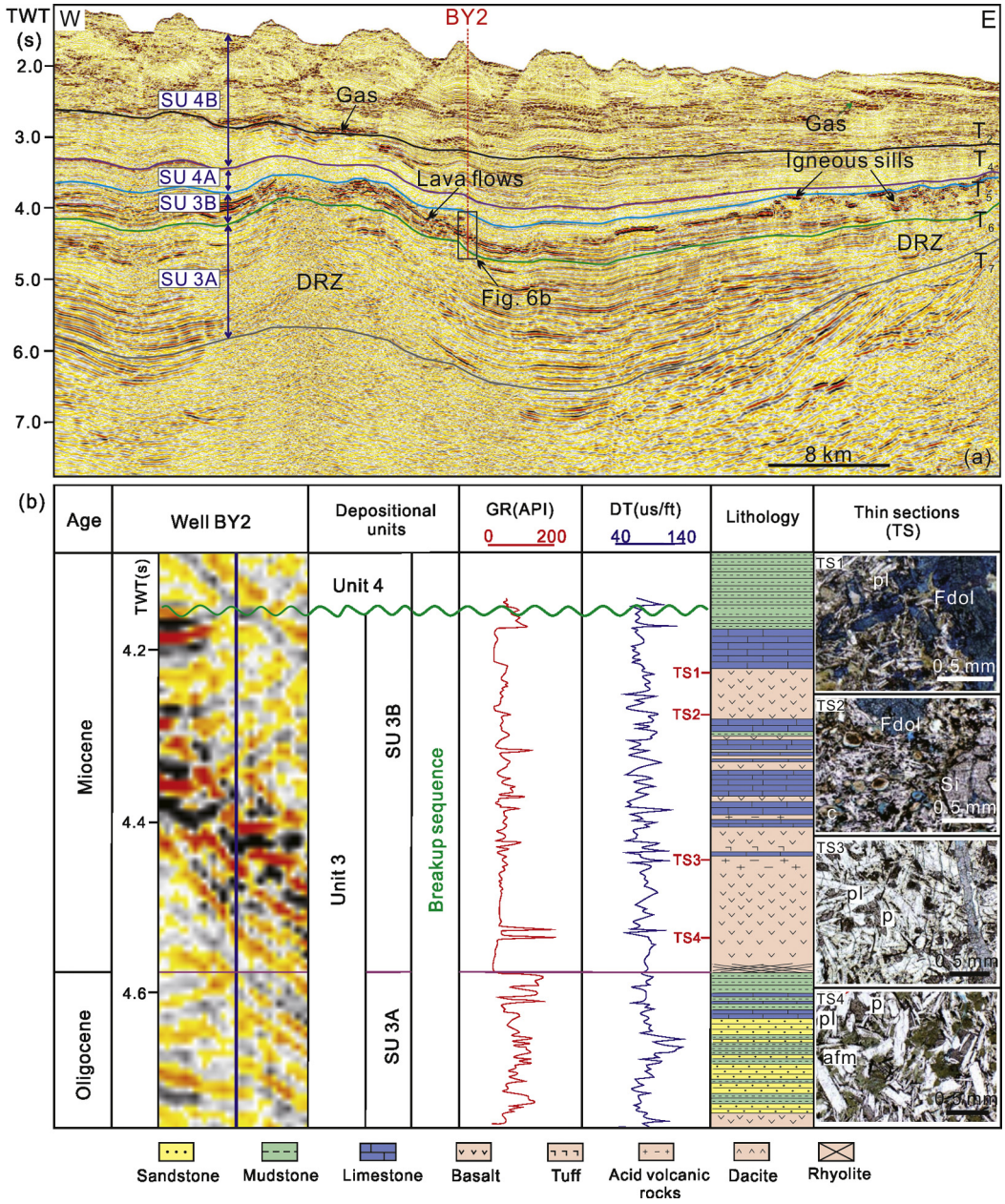

Fig. 6. (a) Seismic section crossing well BY2 which penetrated the eastern flank of a structural high in the Baiyun Sag. Igneous sills, lava flows and shallow gas in Volcanic Complex I are labelled. Gamma-ray (API) and sonic log ($\mu s\,ft^{-1}$) data are shown. See location of the seismic section in Fig. 3b. (b) Correlation panel between well BY2 and seismic section (a) showing the stratigraphic architecture of the breakup sequence. The breakup sequence comprises deltaic to marginal marine sediments, shallow marine volcanic sediments with interbedded carbonate intervals. Photomicrographs show data from four sidewall cores drilled in well BY2 and highlight the severely altered basalt. The locations of photomicrographs from the four sidewall cores are labelled in the figure. Fdol – Fe dolomite; pl – plagioclase; p – pyroxene; Si – siderite; afm – altered ferromagnesian minerals; TS – thin section.

tle folds developed above volcanic mounds result from differential compaction (Figs. 4 and 5).

Mounds form discrete volcanic edifices and are developed between two distinct seismic horizons. In the study area, 26 mounds occur immediately above Horizon T_5 (~18 Ma). Five of these mounds have been interpreted by Zhao et al. (2014), who considered them to be sill-fed volcanic mounds. Two other volcanic mounds occur at the level of Horizon T_6 (~23.8 Ma) (Fig. 4). The consistent observation of onlapping reflections onto the volcanic edifices suggests T_6 and T_5 to represent the seafloor at the time of mound emplacement (Figs. 4 and 5).

A number of discordant, high-amplitude anomalies have saucer-shaped, sheet-shaped, stacked and composite geometries (Figs. 5 and 6). These structures have widths of 0.5 to 12 km and are likely igneous sills similar to those documented on Atlantic continental margins (e.g. Trude et al., 2003; Planke et al., 2005; Figs. 4 to 6). The lateral terminations of several igneous sills coincide with normal faults (S1–4; Figs. 5). In general, the igneous sills observed at shallow depths are imaged either as sub-parallel reflections (S5–11; Fig. 5b) or cross-cutting intrusions (S3; Fig. 5b). Deeper sills are more continuous than the shallower ones, forming concordant intrusions (S1, S3; Fig. 5).

The sheeted or stacked high-amplitude anomalies observed around volcanic mounds are interpreted as lava flows onlapped by overlying strata (Figs. 4–6). As documented in wells BY2 and BY7-1, these lava flows are interbedded with thin-bedded carbonate and siliciclastic intervals. High-amplitude negative anomalies ('soft-on-hard'), which are located directly above lava flows and vertically

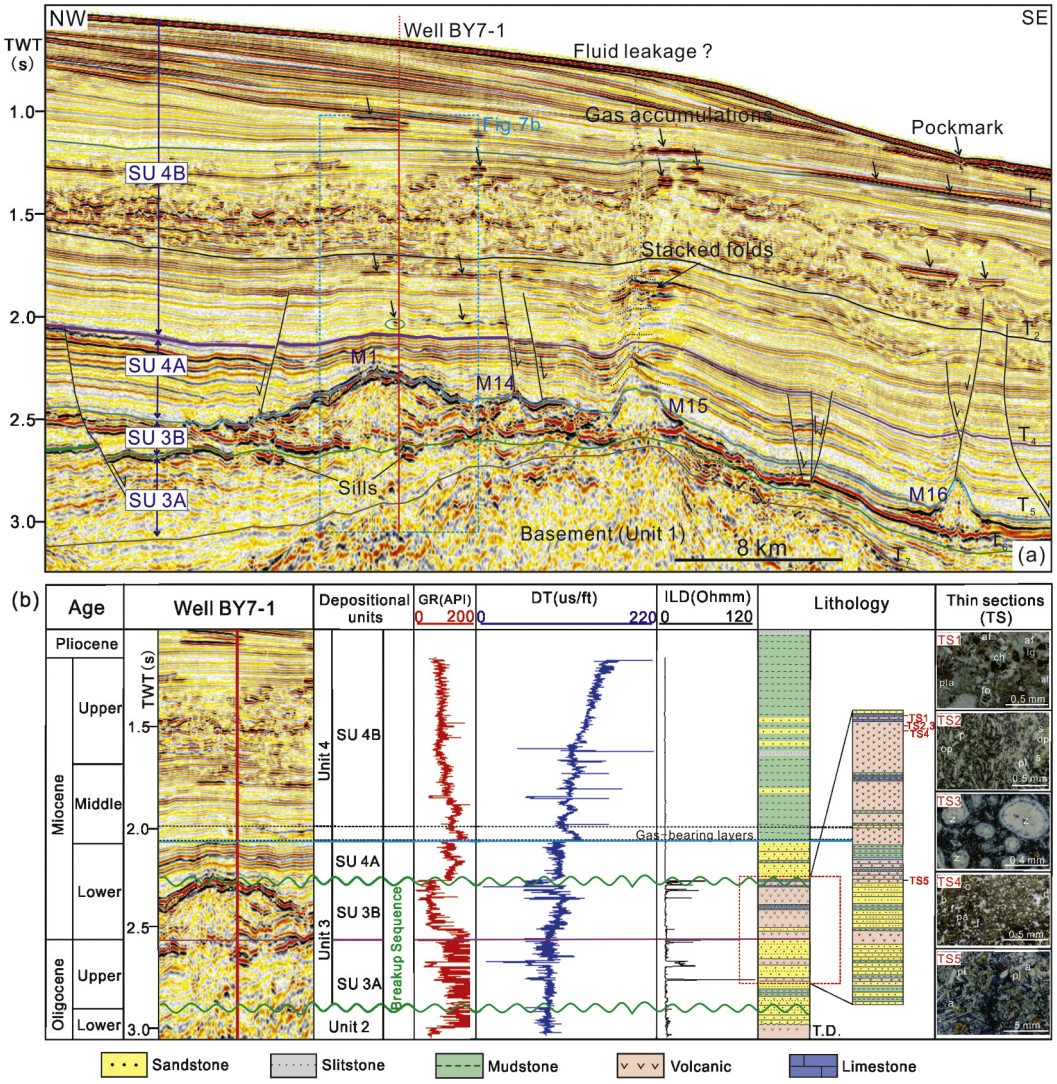

Fig. 7. (a) Interpreted seismic profile showing data from well BY7-1, which penetrated through mound M1. Overburden strata above M15 contain a stack of fold structures and high-amplitude events that terminate upward at Horizon T_2. See Fig. 3b for the location of the seismic profile. (b) Correlation between seismic and borehole data from well BY7-1. To the right are shown photomicrographs from sidewall cores acquired between 2410 and 2845 m through M1. They show biomicrite, olivine basalt, water-rich tuff and augite dolerite. The locations of photomicrographs from five sidewall cores are labeled. af – algal fragment; lg – limonite grain; ch – chlorite; fo – foram; pla – planktic algae; z – zeolite; op – olivine phenocryst; s – serpentine; pl – plagioclase; p – pyroxene; b – basalt; pa – palagonite; f – feldspar; TS – thin section.

connected to Volcanic Complex I by seismic chimneys, have been identified close to Horizon T_2 (Figs. 5 and 6). We interpret them as shallow gas accumulations, trapped in differential compaction folds above the volcanic complex (Figs. 5 and 6).

5.2. Volcanic Complex II

Volcanic Complex II is developed above syn-rift strata and associated basement tilt blocks (Figs. 3, 4, 7 and 8). Volcanic Complex II occurs at a depth between 2000 m and 3500 m below seafloor (c. 3.0 s TWT), and comprises 61 mounds, nine dome-shaped folds and numerous igneous sills (Figs. 3, 4, 7 and 8). Except for M19, mounds in Volcanic Complex II are developed below Horizon T_4 (top of Zhujiang Formation; Figs. 4, 7 and 8). This latter mound is included in Volcanic Complex II as it occurs in the same geographical area.

Mounds in Volcanic Complex II are distinctively sub-circular in plan view (Fig. 8b), and show dome-shaped geometries on seismic profiles (Figs. 4, 7 and 8). They often occur as symmetrical or asymmetrical geometry and have rough flanks. They are 0.5–10 km-wide, 250–710 m-tall and have flank dips of 2°–28°. Their base coincides with a flat-lying, moderate- to high-amplitude positive reflection (BM). On their top is observed a continuous high-amplitude positive reflection (TM) that is clearly onlapped by overlying strata (Figs. 4, 7 and 8). In contrast to the majority of the mounds described in Volcanic Complex II, the top of mounds M15 and M16 comprise low-amplitude negative reflection that are onlapped by adjacent strata (Fig. 7a). This may indicate gas is present in mounds M15 and M16. The internal seismic character of these mounds is complex with chaotic seismic facies that downlap onto the BM surface (Figs. 4, 7 and 8). Mound M19 is distinct from the underlying structures by showing a symmetrical geometry and smooth flanks. This indicates Mound M19 has a different origin and is interpreted as a hydrothermal vent (e.g. Planke et al., 2005; Magee et al., 2013b). Despite being associated with the remainder of Volcanic Complex II, mound M19 was likely emplaced at a later time (Fig. 8).

Fig. 8c shows a coherence slice at 2660 ms (TWT) highlighting the sub-circular shape of volcanic mounds in Volcanic Complex II. The mounds are characterised by low coherence in plan view (Fig. 8c). Fifty of these mounds were developed above or along faults. These faults are observed as NW-trending features with low

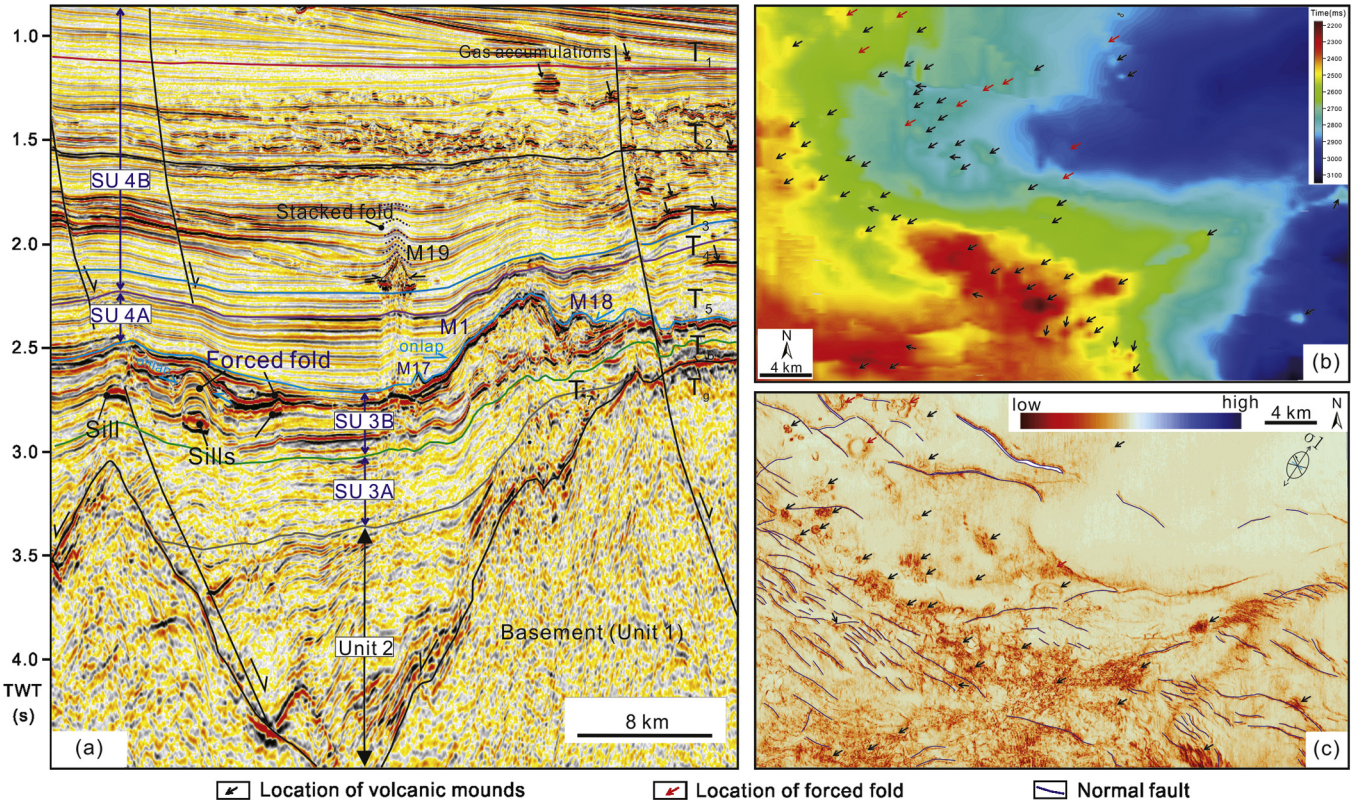

Fig. 8. (a) Stratigraphic correlation along a N–S profile from the Baiyun Sag showing sill-related forced folds and mounds at two distinct stratigraphic levels. Note that most mounded structures occurred above Horizon T_5 (late Early Miocene). In contrast, mound M19 was formed close to Horizon T_3 (Middle Miocene). Normal faults and zones with dimmed reflections are labeled in the figure. See location of the seismic profile in Fig. 3b. (b) Time structure map of the top of Volcanic Complex II at Horizon T_5 illustrating the distribution of volcanic mounds and forced folds. (c) Coherence map from a depth of 2660 ms imaging the volcanic mounds and forced folds at Horizon T_5, towards the western part of the study area. Volcanic mounds and forced folds show low coherence and are highlighted on the map. Numerous faults and fractures are observed within the mounds.

coherence (Fig. 8c). Several vertical chimney structures, recognised as zones of chaotic to low-amplitude reflections, are observed beneath the mounds (Figs. 4, 7 and 8). The strata above Horizon TM is offset by faults that cross the entire section up to T_2 or even T_1, indicating Late Miocene to Pliocene reactivation (Fig. 8).

Nine domal folds occur immediately above the igneous sills and are onlapped by the overlying strata (Figs. 2b and 8). They have diameters of 0.5 to 2.8 km and heights of 140 to 560 m. The spatial extent of the folds closely corresponds to the emplacement of the sills, suggesting a direct relationship between emplaced sills and domal folds. These structures are similar to those identified along the Atlantic margin and are interpreted as forced folds formed by the intrusion of underlying igneous sills (Trude et al., 2003). Strata between Horizon TM and Horizon T_3, above mound M15, is also folded (Fig. 7a). It has been suggested that the folded structures are related to differential compaction (Zhao et al., 2014). Fold angles are steeper close to M15 and become smoother upwards towards Horizon T_2. Bright to chaotic seismic reflections are observed within some of the folds that overlie the volcanic domes, and are interpreted as free gas accumulations (Figs. 7 and 8). The putative occurrence of gas implies that fluid flow into local structural traps occurred after the volcanic mounds were buried.

6. Volcanic complexes at Well BY7-1 and BY2

Two industry wells, BY2 and BY7-1, were drilled in the region where Volcanic Complexes I and II occur (Figs. 3, 4, 6 and 7). Well BY2 drilled vertically stacked lava flows in Volcanic Complex I, within Upper Oligocene to Lower Miocene strata (Fig. 6). Volcanic intervals in well BY2 show P-wave velocities in the range of 3047 m/s to 4688 m/s, and high gamma-ray values (Fig. 6b). An important piece of information is that well BY2 drilled several stratigraphic intervals characterised by basalt lavas and tuffs, which are interbedded with carbonate sediments and terrestrial clastics. These intervals occur at a depth of 4100–4850 m in well BY2 (Fig. 6b). Acidic volcanic rocks, including dacites and rhyolites were encountered at depths of 4490–4500 m, 4515–4540 m and 4820–4850 m (Fig. 6b). Four sidewall core samples were acquired at a depth of 4100–4800 m (Fig. 6). The cores contained altered basalt lavas and tuffs. The principal minerals of the altered volcanic rock are plagioclase, pyroxene and altered ferromagnesian minerals (Fig. 6b). Basalt has been widely replaced by siderite, chert and Fe-dolomite, which fills some of the observed fractures (Fig. 6b).

Well BY7-1 drilled through the eastern part of mound M1, through Pliocene, Upper Miocene and Middle Miocene marine claystones, and Lower Miocene marine sandstones and siltstones (Fig. 7). Well BY7-1 penetrated a 420 m-thick succession of basaltic lavas and tuffs, once again intercalated with thin-bedded limestones and sandstones (Fig. 7b). Below the volcanic deposits were drilled 197 m of Early Miocene sandstones with minor limestones, shales and tuffs (Fig. 7b). Wireline log data suggests the lithology of the mounds is distinct from surrounding sedimentary rocks, with P-wave velocities of 1692–3047 m/s being recorded in sediments vs. 3808–5540 m/s within mound M1 (Fig. 7b). Low gamma ray (GR) and high resistivity values are common in mound M1, with cyclic log responses reflecting multiple extrusive events. In contrast, wireline-log responses for strata above M1 show high P-wave velocities and high gamma ray (GR) values (Fig. 7b).

In mound M1 were drilled eleven limestone layers, intercalated with basaltic lava and ash. Limestone beds consist mainly of encrusting algae, benthic forams, bryozoans, sponge spicules

and scleractinian corals in a micrite matrix, suggesting a shallow-marine depositional environment. Their thickness varies from 0.75 m to 9.0 m. The intercalation of extrusive rocks and sediments suggests that there must have been relatively significant hiatuses in volcanic activity. This observation provides compelling evidence that magmatism is prolonged in the Baiyun Sag during the formation of Volcanic Complexes I and II, as also suggested for the Bight Basin in SW Australia (Magee et al., 2013b). Here, the authors suggested that prolonged magmatism reflected the incremental injection of magma in the plumbing system. We concur with this interpretation for the Baiyun Sag too, particularly within a context of progressive continental breakup and tectonic-plate stress readjustment as the SCS was being formed.

At well BY7-1, five sidewall cores sampled intermediate and basic extrusive rocks within and below mound M1, from 2410 m to 2845 m below the seafloor (Fig. 7b). Sampled rocks consist of altered amygdaloidal basalt lavas and tuffs with lava and basaltic glass fragments (Fig. 7b). Primary minerals of this partially altered basalt are plagioclase, pyroxene, opaque minerals and olivine (Fig. 7b). Zeolite is the main cement and is accompanied by calcite cement in fractures (Figs. 7b). The geochemical analyses reveal that the volcanic rocks in Zhujiang Formation are alkaline basalts with OIB-type geochemical features similar to the dredged basalts from offshore Taiwan (Que et al., 2013; Wang et al., 2012; Lester et al., 2014). Gas-bearing intervals with high water saturations have been identified at 2117 m to 2131 m in Well BY7-1, above Horizon T_5 (Fig. 7a). Wireline data display low P-wave velocities and low gamma-ray values through this same interval (Fig. 7b). These zones are correlated on seismic with negative seismic reflections (i.e. 'soft-on-hard'), which are interpreted as gas accumulations (Fig. 7a).

7. Age and petrographic composition of volcanic mounds and intrusive bodies

At well BY2, no dates are provided for volcanic rocks in Complexes I and II. However, biostratigraphic data from mudstones immediately above and below the volcanic complexes show that lavas and tuffs were erupted in a time period that spans from the Late Oligocene (~24 Ma) to the Early Miocene (~20 Ma). These dates suggest that the lavas and tuffs encountered in well BY2 erupted between 24 Ma and 20 Ma.

The timing of igneous activity in the Baiyun Sag was further constrained at BY7-1 using seismic-borehole ties complemented by nannofossil dating and K–Ar dating methods. The two sidewall cores retrieved from BY7-1 contained nannofossil indicating an Early Miocene age for mound M1. In addition, K–Ar data returned a probable peak age of 17.6 ± 1 Ma for the same two sidewall cores (Yan et al., 2006). A deeper sidewall core was acquired below mound M1, at depth of 3500 m. Estimated K–Ar dates for basalts in this core yielded an age of 35.5 ± 2.8 Ma (Yan et al., 2006). As a result, two volcanic episodes can be recognised in the Baiyun Sag based on well BY7-1: (1) a first episode of explosive volcanism and deposition of tuffs, consistent with a Late Eocene age (~35.5 Ma), and (2) a second episode of voluminous basaltic lava eruptions at ~17.6 Ma (Early Miocene).

The majority of mounds in the second episode formed around 17.6 Ma, bar two (M2 and M11) with an age of ~23.8 Ma (Figs. 4a and 5b). This constrains the relative timing of two igneous episodes between the base of the Early Miocene (T_6) and the late Early Miocene (T_5). The likely origin of these mounds is submarine, with magmatic conduits being fed by basalt magma. The volcanic sequences cored in well BY7-1 display sharp transitions from tuffs to lava flows (Fig. 7b). This character suggests that these sequences formed during magmatic effusive to explosive events. Lateral and vertical facies variations also show sedimentary structures reflecting hiatuses in volcanic eruptions, and suggesting multiple extrusive events (e.g. Magee et al., 2013b).

8. Discussion

8.1. The case for prolonged magmatism during continental breakup

The two volcanic complexes identified in the Baiyun Sag comprise 88 volcanic mounds, multiple igneous sills with associated forced folds (Figs. 4–8). Both intrusive and extrusive features are linked to normal faults and underlying chimney structures, which formed vertical fluid-migration pathways facilitating the transfer of magma towards the surface (Figs. 4–8). Chimney structures are often imaged as zones of chaotic or disrupted seismic reflections, and are likely relate to the presence of igneous dykes (Jaunich, 1983; Svensen et al., 2004; Planke et al., 2005). Subsurface magma flow is closely controlled by pre-existing faults, which comprise both horizontal baffles and preferential vertical pathways for the intrusion of magma (Magee et al., 2013a). In this study, interpreted syn-rift normal faults provide suitable conduits for magma in the Baiyun Sag. A deep-seated mantle plume can be excluded as there is no evidence for such a plume in the SCS. Given evidence from previous studies, the most likely explanation for the occurrence of the Early Miocene alkaline basalts implies from regional lithospheric extension following continental breakup, and onset of seafloor spreading in the SCS (Wang et al., 2012; Lester et al., 2014).

The relative distribution of interbedded extrusive and sedimentary rocks in the Baiyun Sag suggests magmatism in the northern margin of the SCS to reflect a multi-stage evolution, with more than two phases of volcanic activity occurring from the end of the Oligocene. The majority of the investigated mounds were emplaced between T_6 and T_5 (Early Miocene) i.e., they occurred after the onset of continental breakup in the northern SCS (Fig. 4b). Furthermore, the occurrence of two mounds near Horizon T_6 fits well with the onset of seafloor spreading in the Southwest Sub-basin at ~23.6 Ma, based on deep-tow magnetic modelling and microfossil age of recovered cores from IODP Expedition 349 (Li et al., 2014). It has been suggested that Horizon T_6 is the first episode of magmatic activity after continental breakup was initiated, but not fully completed, through the entire SCS (Li et al., 2014). This magmatism was likely induced by regional stress readjustments in the SCS, with subsequent reactivation of pre-existing faults in the Baiyun Sag – which opened up to form conduits for magma sourced from the base of the lithosphere.

Some of the interpreted volcanic mounds show onlap terminations above horizon T_5, a character suggesting that a second episode of magmatic expulsion and reactivation of mound-feeding conduits occurred at the end of the Early Miocene (Fig. 8). Thus, strata between horizons T_7 and T_5 are here correlated with the main period of magmatic activity in the Baiyun Sag, and putatively bound a *breakup sequence sensu* (Soares et al., 2012, 2014) spanning the Early Oligocene–Early Miocene (Figs. 2–7). In contrast, older Late Eocene explosive volcanism is associated syn-rift phase. We suggest that the slow cessation of magmatism observed during continental breakup is due to: a) slow ocean spreading, with the mid-ocean ridge of the SCS, which remained close to the Baiyun Sag after continental breakup due to the complex evolution of the region; b) prolonged rifting and crustal stretching in the northern SCS, with underlying igneous materials using active rift faults to extrude magma onto the surface, or c) upwelling of the asthenosphere during the breakup of northern South China Sea (Fig. 4b).

8.2. Tectono-stratigraphic evolution of the Baiyun Sag during continental breakup

The timing and significance of depositional changes within the Early Oligocene–Early Miocene *breakup sequence* is addressed in

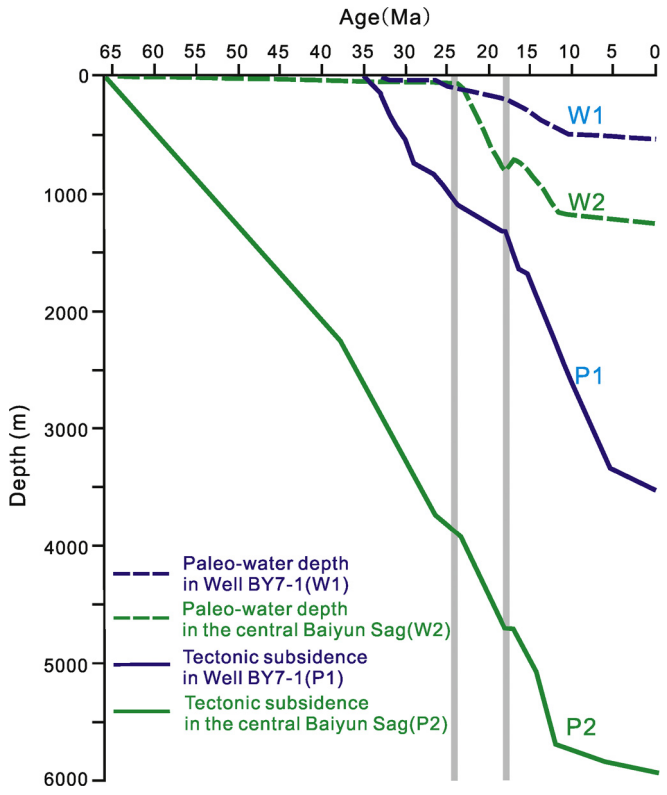

Fig. 9. Subsidence curves for well BY7-1 (P1) and the central Baiyun Sag (P2). Tectonic subsidence at P2 and palaeo-water depth data (W2) are from Xie et al. (2014). For location of the two regions shown see Fig. 3a.

this section (Fig. 10). As previously described, sediments in Unit 3 are deposited in relatively variable tectonic and depositional settings. Subsidence curves for the Baiyun Sag in Xie et al. (2014) reveal significant pre-rift subsidence, whereas the interval between T_7 and T_6 is characterised by moderate subsidence rates (Fig. 9). A period of rapid subsidence period with rates >300 m/My occurred during the deposition of sub-unit 3B and was followed by a decrease in rate of subsidence at ~18 Ma (Fig. 9).

Before 18 Ma, subsidence rates are distinctly variable in the Baiyun Sag. At first, sharp decreases in subsidence rate at ~23 Ma and ~18 Ma suggest that the Baiyun Sag experienced two significant tectonic events (Xie et al., 2014). In contrast, subsidence ensued after the Early Miocene (~18 Ma) as confirmed by the rapid deepening recorded in Fig. 9. Shi et al. (2005) suggested that rapid variations in subsidence rates in the Baiyun Sag were associated with enhanced magmatic activity, an interpretation consistent with the data in this paper.

Along the continental slope of the northern SCS, a series of well-developed submarine canyons document the progressive migration of their axes towards the NE from the Middle Miocene to the present-day (Zhu et al., 2010). It has been suggested that the submarine canyons are associated with the onset of bottom current circulation in the Middle Miocene, reflecting the presence of a fully open basin from this time (e.g. Soares et al., 2014). Palaeobiogeographic evidence from ODP Site 1148 also suggests a strong imprint of bottom current circulation after the Middle Miocene in the SCS (Li et al., 2006), further corroborating this latter interpretation.

Our work recognises distinct depositional units with the *breakup sequence* of the Baiyun Sag (Figs. 3, 6b, 7b and 10). Shallow-marine conditions are recorded in the Baiyun Sag from the onset of continental breakup in the northern part of the SCS (Early Oligocene), and, as documented in this work, the water depth increased from the late Early Miocene onwards. Enhanced igneous activity from T_6 to T_5 favoured the development of shallow-water carbonates during the Early Miocene, particularly over uplifting structural highs. Carbonate intervals also indicate minimal clastic input into the Baiyun Sag at this time. It appears that this decrease in siliciclastic input, and the occurrence of igneous activity, was nearly synchronous in the study area. The T_6 to T_5 interval, in effect, reflects an abrupt switch from siliciclastic to mixed carbonate-siliciclastic deposition, following stratigraphic evidence from ODP Site 1148 (Fig. 2). Here, a rapid increase in $CaCO_3$ above the Oligocene/Miocene boundary suggests high rates of carbonate production in sediment sources from the China mainland (Li et al., 2006).

We consider that the onset of seafloor spreading south of the Baiyun Sag is the most likely factor responsible for the relative sea-level rise recorded in the Early Miocene, generating the accommodation space necessary to enhance carbonate sediment productivity. Local variations in both subsidence rates and lithology during the *breakup sequence* indicate that the Baiyun Sag was tectonically active during the Early Oligocene–Early Miocene. With a continuous rise in sea level, as recorded by the fining upward sediments in sub-unit 4A, carbonate platforms in the SCS were drowned after the end of continental breakup (Fig. 10).

The recognition of significant volcanism within the *breakup sequence* takes into account the tectonic and sedimentological changes observed during continental breakup in the SCS. The deposition of the breakup sequence suggests that important changes in terms of magma emplacement and depositional environment occurred after the continental breakup event was initiated. In addition, we suggest that important changes in oceanic circulation occurred after continental breakup was established throughout the entire SCS, with the record of such changes being preserved in the migrating submarine canyon systems developed on the continental slope.

9. Conclusions

New high-resolution 3D seismic data were used to investigate the origin of two volcanic complexes in the deep-offshore Baiyun Sag, south of the Pearl River Mouth Basin. The observed volcanic complexes include eighty-eight (88) volcanic mounds, numerous igneous sills and lava flows. Petrological analyses from borehole sidewall cores suggest the volcanic mounds comprise basalt lavas and tuffs intercalated with thin-bedded limestone and clastic beds. The basaltic lavas are hydrothermally altered. The limestone intervals penetrated within mound M1 and associated lava flows show the two volcanic complexes were generated during multiple extrusion events. The occurrence of intrusive and extrusive features is indicative of magma expulsion at the seafloor and represents a chronological marker for the timing of magmatic activity.

Nannofossil and K–Ar data obtained from sidewall cores drilled in Volcanic Complexes I and II suggest that magma emplacement occurred in multiple events during the Miocene. Therefore, the study area is an example of moderate magmatism occurring as continental breakup progressed in the SCS from NE to SW. As a result, volcanism in the Baiyun Sag occurred during continental breakup in two major stages: (1) two volcanic mounds formed near Horizon T_6 (Oligocene/Miocene boundary), and are associated with the onset of seafloor spreading in Southwest Sub-basin; (2) eight-six (86) volcanic mounds and numerous igneous sills dated as Early Miocene are clearly associated with continental breakup in the SCS, extending to the top of a putative *break-up sequence* in the Baiyun Sag.

This study provides evidence that the continental breakup initiates important changes in the depositional architecture of continental margins, within a well-defined *breakup sequence*. The sedimentological changes recorded in the Baiyun Sag reflect a

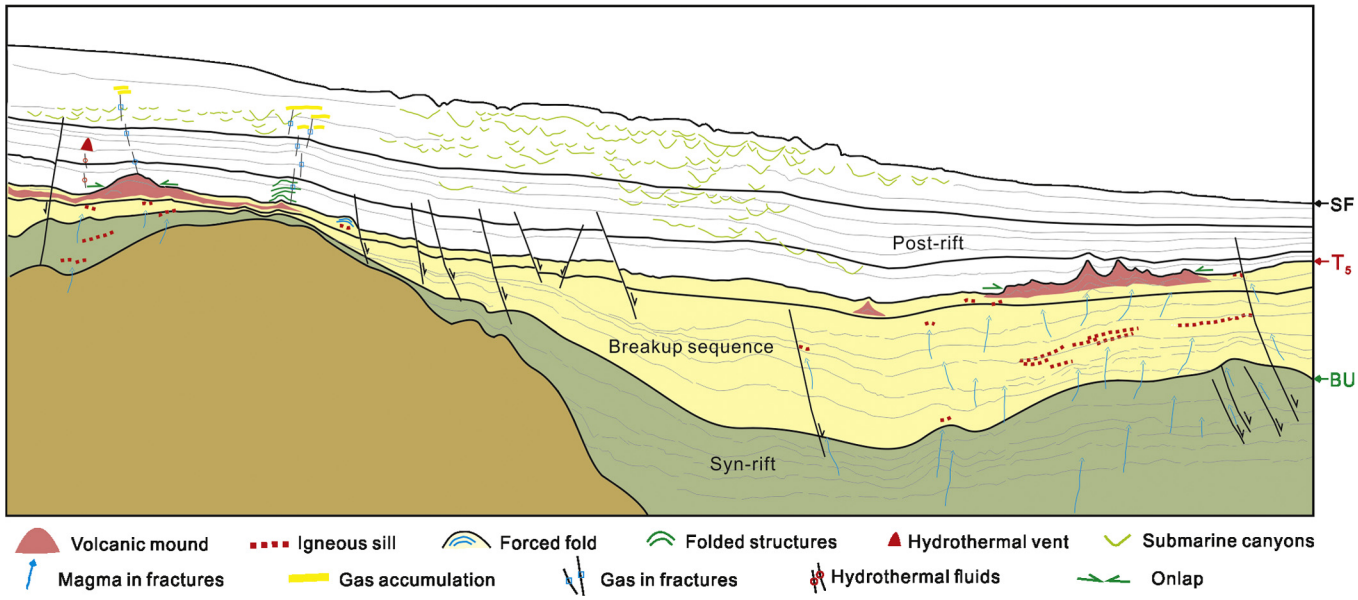

Fig. 10. Schematic illustration showing the formation of igneous complexes in relation to the Early Oligocene–Early Miocene breakup sequence of the Baiyun Sag. SF – Seafloor; BU – Breakup unconformity.

tectonically active environment during the development of an Early Oligocene–Early Miocene *breakup sequence*. As a corollary, the onset of deep-water circulation recorded after the *breakup sequence* marks the establishment of oceanic circulation in the newly formed South China Sea.

Acknowledgements

This study was supported by the Fundamental Research Program of the Ministry of Sciences and Technology, China (No. 2015CB251201), the National Natural Science Foundation of China (Nos. 91228208 and 91328206), and the Knowledge Innovation Project of the Sanya Institute of Deep Sea Sciences and Engineering (No. SIDSSE-201403). We thank China National Offshore Oil Company for providing the data and permission to publish this paper. We would like to thank T.A. Minshull for his constructive comments, which greatly improved this paper. The editor P. Shearer and reviewers C. Magee and D. Iacoppini are acknowledged for their helpful reviews.

References

Briais, A., Patriat, P., Tapponnier, P., 1993. Updated interpretation of magnetic anomalies and seafloor spreading stages in the South China Sea: implications for the Tertiary tectonics of Southeast Asia. J. Geophys. Res. 98, 6299–6328.

Brown, A., 2004. Interpretation of Three-Dimensional Seismic Data, 7th edn. AAPG Mem., vol. 42.

Ding, W.W., Li, J.B., Dong, C.Z., Fang, Y.X., 2015. Oligocene–Miocene carbonates in the Reed Bank area, South China Sea, and their tectono-sedimentary evolution. Mar. Geophys. Res. 36, 149–165.

Falvey, D.A., 1974. The development of continental margins in plate tectonic theory. APPEA J. 14, 95–107.

Franke, D., 2013. Rifting, lithosphere breakup and volcanism: comparison of magma-poor and volcanic rifted margins. Mar. Pet. Geol. 43, 63–87.

Gao, J., Wu, S., McIntosh, K., Mi, L., Yao, B., Chen, Z., Jia, L., 2015. The continent–ocean transition at the mid-northern margin of the South China Sea. Tectonophysics 654, 1–19.

Hale, D., 2013. Methods to compute fault images, extract fault surfaces, and estimate fault throws from 3D seismic images. Geophysics 78, O33–O43.

Hu, D., Zhou, D., Wu, X., He, M., Pang, X., Wang, Y., 2009. Crustal structure and extension from slope to deepsea basin in the northern South China Sea. J. Earth Sci. 20, 27–37.

Huismans, R.S., Beaumont, C., 2008. Complex rifted continental margins explained by dynamical models of depth dependent lithospheric extension. Geology 36, 163–166.

Jaunich, S., 1983. Tertiary intrusions on the south-western African margin. In: Bally, A.W. (Ed.), Seismic Expression of Structural styles. In: AAPG Stud. Geol. 1, vol. 15. Am. Assoc. Petrol. Geol., Tulsa, OK, pp. 10–14. Section 1.3.

Kyrkjebø, R., Gabrielsen, R.H., Faleide, J.I., 2004. Unconformities related to the Jurassic–Cretaceous synrift–post-rift transition of the northern North Sea. J. Geol. Soc. (Lond.) 161, 1–17.

Lester, R., Van Avendonk, H.J.A., McIntosh, K., Lavier, L., Liu, C.-S., Wang, T.K., Wu, F., 2014. Rifting and magmatism in the northeastern South China Sea from wide-angle tomography and seismic reflection imaging. J. Geophys. Res., Solid Earth 119 (3), 2305–2323.

Li, P.L., Rao, C.T., 1994. Tectonic characteristics and evolution history of the Pearl River mouth basin. Tectonophysics 235, 13–25.

Li, C.-F., Lin, J., Kulhanek, D.K., 2013. South China Sea tectonics: opening of the South China Sea and its implications for southeast Asian tectonics, climates, and deep mantle processes since the late Mesozoic. IODP Sci. Prosp. 349. http://dx.doi.org/10.2204/iodp.sp.349.2013.

Li, C.F., Xu, X., Lin, J., Sun, Z., et al., 2014. Ages and magnetic structures of the South China Sea constrained by the deep tow magnetic surveys and IODP Expedition 349. Geochem. Geophys. Geosyst. 15, 4958–4983.

Li, Q., Wang, P., Zhao, Q., Shao, L., Zhong, G., Tian, J., Cheng, X., Jian, Z., Su, X., 2006. 33 Ma lithostratigraphic record of tectonic and paleoceanographic evolution of the south China sea. Mar. Geol. 230, 217–235.

Lin, A.T., Watts, A.B., Hesselbo, S.P., 2003. Cenozoic stratigraphy and subsidence history of the South China Sea margin in the Taiwan region. Basin Res. 15, 453–478.

Lister, G.S., Etheridge, M.A., Symonds, P.A., 1986. Detachment faulting and the evolution of passive continental margins. Geology 14, 246–250. http://dx.doi.org/10.1130/0091-7613.

Lüdmann, T., Wong, H., 1999. Neo-tectonic regime on the passive continental margin of the northern South China Sea. Tectonophysics 311, 113–138.

Magee, C., Jackson, C.A.-L., Schofield, N., 2013a. The influence of normal fault geometry on igneous sill emplacement and morphology. Geology 41, 407–410.

Magee, C., Hunt-Stewart, E., Jackson, C.A.-L., 2013b. Volcano growth mechanism and the role of sub-volcano intrusions: insight from 2D seismic reflection data. Earth Planet. Sci. Lett. 373, 41–53.

Manatschal, G., Bernoulli, D., 1999. Architecture and tectonic evolution of nonvolcanic margins: present day Galicia and ancient Adria. Tectonics 18, 1099–1119.

Mutter, J.C., Talwani, M., Stoffa, P.L., 1982. Origin of seaward-dipping reflectors in oceanic crust off the Norwegian margin by "subaerial sea-floor spreading". Geology 10, 353–357.

Nissen, S.S., Hayes, D.E., Buhl, P., Diebold, J., Bochu, Y., Weijun, Z., Yongqin, C., 1995. Deep penetration seismic soundings across the northern margin of the South China Sea. J. Geophys. Res. 100 (B11), 22407–22433.

Pindell, J., Graham, R., Horn, B., 2014. Rapid outer marginal collapse at the rift to drift transition of passive margin evolution, with a Gulf of Mexico case study. Basin Res. 26, 701–725.

Planke, S., Rasmussen, T., Rey, S.S., Myklebust, R., 2005. Seismic characteristics and distribution of volcanic intrusions and hydrothermal vent complexes in the Vøring and Møre basins. In: Dore, A.G., Vining, B.A. (Eds.), Petroleum Geology: North-West Europe and Global Perspectives—Proceedings of the 6th Petroleum

Geology Conference. Petroleum Geology Conferences Ltd. Published by the Geological Society, London, pp. 833–844.
Que, X.M., Li, Y.S., Chen, H.X., Zhang, Q.L., Zhang, X.T., 2013. Geochemistry research on the deep mantle activity in Baiyun Sag during the Cenozoic from the volcanic rocks of well BY7. Geology and Mineral Resources of South China 29 (2), 105–115 (in Chinese with English abstract).
Reston, T., 2007. Extension discrepancy at North Atlantic nonvolcanic rifted margins: depth-dependent stretching or unrecognized faulting? Geology 35, 367–370.
Shi, X., Burov, E., Leroy, S., Qiu, X., Xia, B., 2005. Intrusion and its implication for subsidence: a case from the Baiyun Sag, on the northern margin of the South China Sea. Tectonophysics 407, 117–134.
Skogly, O.P., 1998. Seismic characterisation and emplacement in the Voring basin. M.Sc. thesis. University of Oslo.
Soares, D.M., Alves, T.M., Terrinha, P., 2012. The breakup sequence and associated lithospheric breakup surface: their significance in the context of rifted continental margins (West Iberia and Newfoundland margins, North Atlantic). Earth Planet. Sci. Lett. 355–356, 311–326.
Soares, D.M., Alves, T.M., Terrinha, P., 2014. Contourite drifts on the early passive margins as an indicator of established lithospheric breakup. Earth Planet. Sci. Lett. 401, 116–131.
Sun, Z., Zhou, D., Pang, X., Huang, C.J., Chen, C.M., Zhong, Z.H., He, M., Xu, H.H., 2008. Dynamics analysis of the Baiyun Sag in the Pearl River Mouth basin, North of South China Sea. Acta Geol. Sin. 82 (1), 73–83.
Sun, Z., Xu, Z., Sun, L., Pang, X., Yan, C., Li, Y., Zhao, Z., Wang, Z., Zhang, C., 2014a. The mechanism of post-rift fault activities in Baiyun sag, Pearl River Mouth basin. J. Asian Earth Sci. 89, 76–87.
Sun, Q.L., Wu, S.G., Cartwright, J., Wang, S.H., Lu, Y.T., Chen, D.X., Dong, D.D., 2014b. Neogene igneous intrusions in the northern South China Sea: evidence from high resolution three dimensional seismic data. Mar. Pet. Geol. 54, 83–95.
Svensen, H., Planke, S., Malthe-Sørensen, A., Jamtveit, B., Myklebust, R., Eidem, T.R., Rey, S.S., 2004. Release of methane from a volcanic basin as a mechanism for initial Eocene global warming. Nature 429, 542–545.
Taylor, B., Hayes, D.E., 1983. Origin and history of the South China Sea Basin. In: Hayes, D.E. (Ed.), The Tectonic and Geologic Evolution of Southeast Asian Seas and Islands Part 2. In: Geophys. Monogr., vol. 27. Am. Geophys. Union, pp. 23–56.
Trude, J., Cartwright, J., Davies, R.J., Smallwood, J., 2003. New technique for dating igneous sills. Geology 31, 813–816.
Wang, K.-L., Lo, Y.-M., Chung, S.-L., Lo, C.-H., Hsu, H.K., Yang, H.-J., Shinjo, R., 2012. Age and geochemical features of dredged basalts from offshore SW Taiwan: the coincidence of intra-plate magmatism with the spreading South China Sea. Terr. Atmos. Ocean. Sci. 23 (6), 657–669.
Wang, P., Prell, W.L., Blum, P., Arnold, E.M., Buehring, C.J., Chen, M.-P., Clemens, S.C., Clift, P.D., Colin, C.J.G., Farrell, J.W., Higginson, M.J., Jian, Z., Kuhnt, W., Laj, C.E., LauerLeredde, C., Leventhal, J.S., Li, A., Li, Q., Lin, J., McIntyre, K., Miranda, C.R., Nathan, S.A., Shyu, J.-P., Solheid, P.A., Su, X., Tamburini, F., Trentesaux, A., Wang, L., 2000. Ocean Drill. Program Proc., Initial Rep., vol. 184. Ocean Drilling Program, College Station, TX.
Wang, T., Chen, M., Lee, C., Xia, K., 2006. Seismic imaging of the transitional crust across the northeastern margin of the South China Sea. Tectonophysics 412, 237–254.
White, R., McKenzie, D., 1989. Magmatism at the rift zones: the generation of volcanic continental margins and flood basalts. J. Geophys. Res. 94, 7685–7729.
Whitmarsh, R.B., Manatschal, G., Minshull, T.A., 2001. Evolution of magma-poor continental margins from rifting to seafloor spreading. Nature 413, 150–154.
Whitmarsh, R.B., Wallace, P.J., 2001. The rift-to-drift development of the West Iberia nonvolcanic margin: a summary and review of the contribution of Ocean Drilling Project Leg 173. In: Beslier, M.-O., Whitmarsh, R.B., Wallace, P.J., Girardeau, J. (Eds.), Ocean Drill. Program Proc., Sci. Results, vol. 173. Ocean Drilling Project, College Station, TX, pp. 1–36.
Withjack, M.O., Schlische, R.W., Olsen, P.E., 1998. Diachronous rifting, drifting, and inversion on the passive margin of Central Eastern North America: an analog for other passive margins. AAPG Bull. 82, 817–835.
Xie, H., Zhou, D., Li, Y.P., Pang, X., Li, P.X., Chen, G.H., Li, F.C., Cao, J.H., 2014. Cenozoic tectonic subsidence in deepwater sags in the Pearl River Mouth Basin, northern South China Sea. Tectonophysics 615–616, 182–198.
Yan, P., Deng, H., Liu, H., Zhang, Z., Jiang, Y., 2006. The temporal and spatial distribution of volcanism in the South China Sea region. J. Asian Earth Sci. 27, 647–659.
Yu, H.S., 1994. Structure, stratigraphy and basin subsidence of Tertiary basins along the Chinese southeastern continental margin. Tectonophysics 253, 63–76.
Zhao, F., Wu, S.G., Sun, Q.L., Huuse, M., Li, W., Wang, Z.J., 2014. Submarine volcanic mounds in the Pearl River Mouth Basin, northern South China Sea. Mar. Geol. 355, 162–172.
Zhou, D., Ru, K., Chen, H.-Z., 1995. Kinematics of Cenozoic extension on the South China Sea continental margin and its implications for the tectonic evolution of the region. Cenozoic tectonic subsidence in deepwater sags in the Pearl River Mouth Basin, northern South China Sea. Tectonophysics 251, 161–177.
Zhu, M.Z., Graham, S., Pang, X., McHargue, T., 2010. Characteristics of migrating submarine canyons from the middle Miocene to present: implications for paleoceanographic circulation, northern South China Sea. Mar. Pet. Geol. 27, 307–319.